Geochemistry, Geophysics, Geosystems

RESEARCH ARTICLE
10.1029/2018GC007506

No Measurable Calcium Isotopic Fractionation During Crystallization of Kilauea Iki Lava Lake

Hongming Zhang[1,2,3], Yang Wang[2], Yongsheng He[2], Fang-Zhen Teng[4], Stein B. Jacobsen[3], Rosalind T. Helz[5], Bruce D. Marsh[6], and Shichun Huang[7]

[1]State Key Laboratory of Continental Dynamics, Department of Geology, Northwest University, Xi'an, China, [2]State Key Laboratory of Geological Processes and Mineral Resources, China University of Geosciences, Beijing, China, [3]Department of Earth and Planetary Sciences, Harvard University, Cambridge, MA, USA, [4]Department of Earth and Space Sciences, University of Washington, Seattle, WA, USA, [5]United States Geological Survey, Reston, VA, USA, [6]Department of Earth and Planetary Science, Johns Hopkins University, Baltimore, MD, USA, [7]Department of Geoscience, University of Nevada, Las Vegas, Las Vegas, NV, USA

Abstract In order to investigate possible Ca isotopic fractionation during basaltic magma differentiation, we measured Ca isotopic compositions of lavas recovered from Kilauea Iki lava lake at Hawaii. This set of lavas record the whole crystal fractionation history of basaltic magma, ranging from olivine accumulation/fractionation to multiple phase crystallization, including plagioclase and clinopyroxene. Our results show no detectable Ca isotopic variation in all measured Kilauea lavas at a precision of ±0.07‰ for $^{44}Ca/^{40}Ca$ ($\delta^{44/40}Ca = 0.80 \pm 0.08$, 2 SD, $n = 19$). Using such observation and published intermineral Ca isotopic fractionation factors, a Monte Carlo approach is used to estimate the mineral-melt $^{44}Ca/^{40}Ca$ fractionation factors. We found that Ca isotopic fractionation between clinopyroxene and basaltic melt is small, with $\Delta^{44/40}Ca^{cpx\text{-}melt} = 0.04 \pm 0.03$ at 1200 °C. To the best of our knowledge, this is the first estimated mineral-melt Ca isotopic fractionation factor reported. We use this estimated $\Delta^{44/40}Ca^{cpx\text{-}melt}$ and intermineral Ca isotopic fractionation factors to investigate Ca isotopic effects during mantle partial melting under 1–2 GPa. Our simulations show that the largest $^{44}Ca/^{40}Ca$ effect, up to +0.3‰, is achieved in large degree melting residues during fractional and dynamic melting. In contrast, partial melts show negligible $^{44}Ca/^{40}Ca$ isotopic effect, <0.07‰.

Key Points:
- Kilauea Iki lava lake basalts show no detectable Ca isotopic variation at a precision of ±0.07‰ for $^{44}Ca/^{40}Ca$
- The clinopyroxene-melt Ca isotopic fractionation factor is estimated at (0.09 ± 0.07)/(T/1,000)2 (T in kelvin)
- Small $^{44}Ca/^{40}Ca$ fractionation in melts during crystal fractionation and melting of spinel peridotite, but large $^{44}Ca/^{40}Ca$ (0.3‰) fractionation in residues

Supporting Information:
- Supporting Information S1
- Table S1
- Table S2
- Table S3
- Table S4
- Table S5
- Table S6
- Table S7
- Table S8
- Figure S1
- Figure S2
- Figure S3

Correspondence to:
H. Zhang and S. Huang,
hongmingzhang@aliyun.com;
shichun.huang@unlv.edu

Citation:
Zhang, H., Wang, Y., He, Y., Teng, F.-Z., Jacobsen, S. B., Helz, R. T., et al. (2018). No measurable calcium isotopic fractionation during crystallization of Kilauea Iki lava lake. *Geochemistry, Geophysics, Geosystems*, *19*, 3128–3139. https://doi.org/10.1029/2018GC007506

Received 23 FEB 2018
Accepted 27 JUL 2018
Accepted article online 18 AUG 2018
Published online 14 SEP 2018

1. Introduction

Calcium is the fifth most abundant element in the Earth, with six stable isotopes ranging from 40 to 48 (Coplen et al., 2002). Recent studies show large mass-dependent Ca isotopic variations in silicate rocks with $\delta^{44/40}Ca$ ($\delta^{44/40}Ca = [(^{44}Ca/^{40}Ca)_{sample}/(^{44}Ca/^{40}Ca)_{NIST915a} - 1] \times 1{,}000$) ranging from −0.08 to 1.68 (Figures 1 and S1). What causes such large Ca isotopic variations in silicate rocks?

Some of the variation in silicate rocks may reflect interlab difference (see He et al. 2017, Figure 8). For example, the reported $\delta^{44/40}Ca$ values for USGS standard sample DTS-1 range from 1.49 to 1.68 (Figure 1). However, the large $\delta^{44/40}Ca$ variation in igneous rocks is not only a result of large interlab difference. Several mechanisms have been proposed for the observed Ca isotopic variation in silicate rocks (Figure 1): (1) some reflect equilibrium isotopic fractionation during magmatic processes (Feng et al., 2014; Huang et al., 2010; Kang et al., 2016), (2) some are attributed to the recycling of surface material into the deep mantle (Huang et al., 2011), (3) some might reflect kinetic isotopic effect during melt-rock reactions (Zhao et al., 2017), and (4) some may be attributed to low-temperature alteration effects (such the high $\delta^{44/40}Ca$ in DTS-1; Huang et al., 2010). Knowledge about the Ca isotopic effects produced by magmatic processes is required to use $\delta^{44/40}Ca$ as an important geochemical tracer in the field of mantle geochemistry and igneous petrology.

In this paper, we attempt to constrain the Ca isotopic fractionation behavior during basalt crystal fractionation and mantle partial melting processes, two important processes that produce the geochemical variations in basalts. Amini et al. (2009) observed large $\delta^{44/40}Ca$ variation in igneous rocks ($\delta^{44/40}Ca$ = 0.61–1.49, n = 22), and proposed that partial melting and crystal fractionation may be responsible for the observed large $\delta^{44/40}Ca$ variation. However, due to the lack of knowledge of mineral-melt Ca isotopic fractionation factors, they were not able to evaluate the Ca isotopic effects caused by these two processes. Based on the large Ca isotopic fractionation between coexisting orthopyroxene and clinopyroxene in

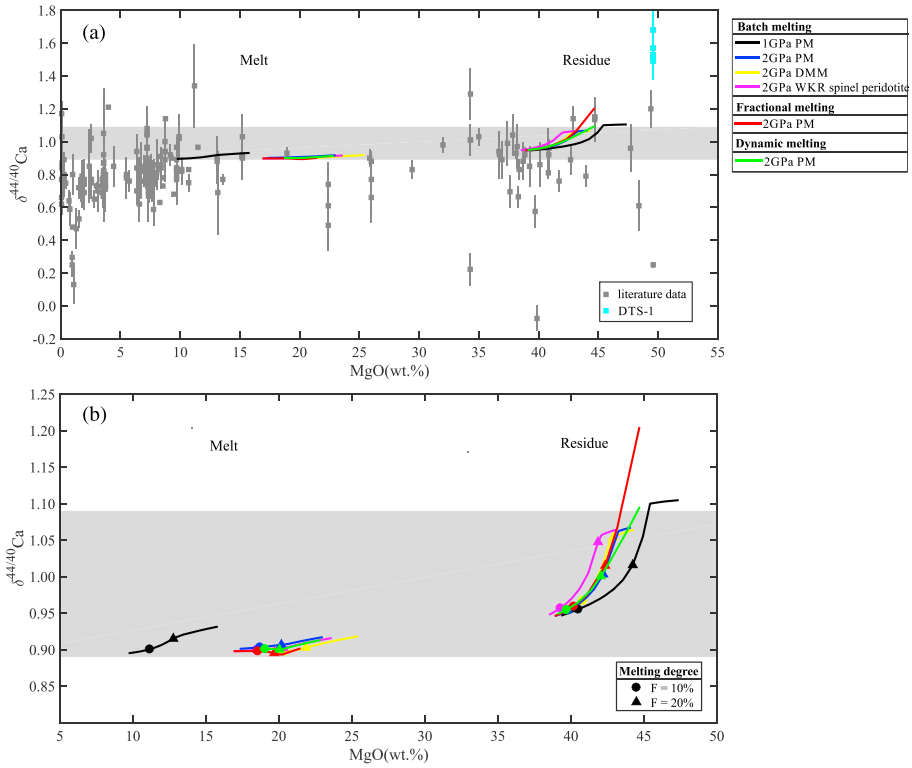

Figure 1. (a) Plot of whole-rock $\delta^{44/40}$Ca against MgO content for igneous rocks (gray squares; see Table S3 for data compilation; Amini et al., 2009; Colla et al., 2013; DePaolo, 2004; Fantle & Tipper, 2014; Feng et al., 2017; He et al., 2017; Holmden & Bélanger, 2010; Huang et al., 2010, 2011; Jacobson et al., 2015; Jochum et al., 2006; John et al., 2012; Kang et al., 2016, 2017; Lehn & Jacobson, 2015; Liu, Li, et al., 2017; Liu, Zhu, et al., 2017; Magna et al., 2015; Richter et al., 2003; Ryu et al., 2011; Schiller et al., 2012; Simon & DePaolo, 2010; Simon et al., 2017; Skulan et al., 1997; Valdes et al., 2014; Wombacher et al., 2009; Zhao et al., 2017; Zhu et al., 2018; Zhu & Macdougall, 1998). It is evident that interlab difference contributes to some of the variation in silicate rocks (see He et al. 2017, Figure 8). For example, the reported $\delta^{44/40}$Ca values for USGS standard samples DTS-1 range from 1.49 to 1.68, highlighted as cyan squares. Lines are our model results of Ca isotopic variations in melts (MgO $<$ 25 wt %) and residues (MgO $>$ 25 wt %) produced by mantle partial melting under 1 to 2 GPa (see detailed discussion in section 5.3). The horizontal gray band represents the suggested BSE Ca isotopic composition ($\delta^{44/40}$Ca = 0.89 to 1.09; Huang et al., 2010; Kang et al., 2017; Simon & DePaolo, 2010). Plot of whole-rock $\delta^{44/40}$Ca against CaO content for igneous rocks and model lines are shown in Figure S1. (b) Plot of $\delta^{44/40}$Ca in melts and residues from our simulations (section 5.3) with expanded *y* axis. The degrees of partial melting range from 5 to 30%, and 10 and 20% tick marks are labeled in each model lines. The inflection points on the batch melting residue trends are where clinopyroxene is completely consumed (Table S6).

mantle peridotites ($\Delta^{44/40}Ca^{opx\text{-}cpx}$ = 0.36–0.75), Huang et al. (2010) suggested that Ca isotopes might be fractionated during partial melting process. This idea has been shared by several recent publications (Kang et al., 2016, 2017; Zhu et al., 2018). Using arbitrarily selected peridotite-melt Ca isotopic fractionation factors ($\Delta^{44/40}Ca^{peridotite\text{-}melt}$ = 0.10–0.25), Kang et al. (2016, 2017) argued that the high $\delta^{44/40}$Ca in some peridotites, up to 1.5, which is significantly higher than bulk silicate Earth estimate of 0.89 to 1.09 (Figure 1; Huang et al., 2010; Kang et al., 2017; Simon & DePaolo, 2010), can be produced by large degrees (*F* = ~25–30%) of partial melting. As another example, Zhu et al. (2018) reported low $\delta^{44/40}$Ca, 0.75–0.86, in N-MORB from southern Juan de Fuca ridge. Following the same approach of Kang et al. (2017), Zhu et al. (2018) argued that the observed low $\delta^{44/40}$Ca in N-MORB is caused by mantle partial melting.

The peridotite-melt Ca isotopic fractionation factor is important in understanding Ca isotopic fractionation during partial melting. However, the peridotite-melt Ca isotopic fractionation factor has not been determined by experiments or theoretical calculations (Kang et al., 2017). Equilibrium intermineral Ca isotopic fractionation has been systematically studied using first-principles calculations (Feng et al., 2014; Wang et al., 2017; Zhou et al., 2016); however, such approach has not been extended to calculate the mineral-melt isotopic fractionation. In this paper, we will take a different approach to attack this problem by using a

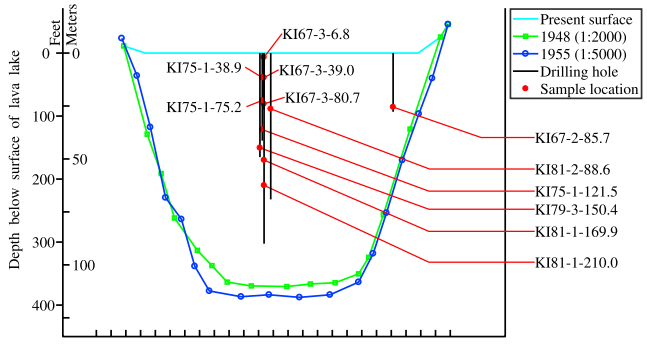

Figure 2. Cross section of Kilauea Iki lava lake. The present surface (cyan line) of the lava lake and two preeruption profiles are shown from two different topographic maps: one (at 1:2,000, green line) is based on aerial photographs taken in 1948 and the other (at 1:5,000, blue line) is based on aerial photographs taken in 1955. Sample locations are shown as red circles with their names labeled. Vertical exaggeration is 4:1. After Helz (2012).

combination of Ca isotopic measurements of natural basalts and intermineral Ca isotopic fractionation factors obtained from first-principles calculations and an ionic model. A similar method was used by Sossi et al. (2012) to study the Fe isotopic variations in the Red Hill intrusion in southern Tasmania.

Basalts from Kilauea Iki lava lake, Hawaii, USA, were produced by closed-system crystal-melt fractionation, and their crystal fractionation history is well recorded (Helz, 1987). Combined with intermineral Ca isotopic fractionation factors, involving clinopyroxene, pigeonite, and plagioclase, $\delta^{44/40}$Ca data of Kilauea Iki lava lake basalts allow us to calculate the mineral-melt Ca isotopic fractionation factors using mass balance relationships. Then, we will apply these mineral-melt Ca isotopic fractionation factors to constrain possible Ca isotopic effects during mantle melting. Our results provide a first-order "roadmap" to use Ca isotopes in the field of petrology and mantle geochemistry, and it must be checked with future studies using high-temperature experiments.

2. Geological Settings and Samples

Kilauea Iki lava lake was formed during the 1959 summit eruption of Kilauea volcano located in the southeast of Hawaii Island (Figure 2). This lava lake is a perfect place for studying magma differentiation, because it cooled and crystallized as a closed system from 1960 to the mid-1990s. At the same time, the interior was sampled by coring from the surface of the lake to the bottom. Its crystallization sequence and thermal history have been well recorded (Helz, 1987, 2012; Helz & Thornber, 1987; Teng et al., 2011). Their major and trace element contents, and other stable isotopic compositions, such as Li, Mg, Fe, Si, Zn, and Ga, have been well studied (Chen et al., 2013; Greaney et al., 2017; Helz, 2012; Helz et al., 1994; Kato et al., 2017; Pitcher et al., 2009; Teng et al., 2007, 2008, 2010, 2011; Tomascak et al., 1999). Some elements (Fe, Si, Zn) show detectable whole-rock isotopic variations, while others (Li, Mg, Ga) do not.

Magma differentiation of Kilauea Iki lava lake magma has created a variety of rock types, ranging from olivine-rich cumulates, through olivine tholeiites, to ferrodiabase and more silicic veins, with MgO contents decreasing from 27.41 to 2.37 wt %. CaO contents increased from 5.21 to 12.30 wt % and then decreased to 6.08 wt %. Samples studied include two scoriae from a fire fountain (Iki-22 and Iki-58) and eleven drill core samples from the interior of the lake. A detailed description of these Kilauea Iki samples is given in Pitcher et al. (2009). The scoriae consist of olivine phenocrysts and glass. Most core samples are olivine-phyric basalts. Other core samples with low MgO content (<5 wt %) are differentiated segregation veins. Sample KI75–1-75.2 is a ferrodiabase segregation vein. Two samples, KI67–2-85.7 and KI81–2-88.6, formed from melt found within segregation veins that had partly crystallized. USGS standard samples, BHVO-1 and -2, which are from the Kilauea 1919 eruption, were also included. We also analyzed one Kilauea dacite sample (the Puna dacite; Teplow et al., 2009). This sample was recovered as a dacite melt at the Puna Geothermal Venture Wellfield. It has low MgO content (2.29 wt %) relative to other Kilauea Iki samples and is interpreted as the final product of fractional crystallization of the magma from Kilauea.

3. Analytical Methods

Calcium isotopic analyses were performed at China University of Geosciences, Beijing. Detailed Ca isotopic analytical procedure at China University of Geosciences, Beijing, was reported in He et al. (2017). Sample powders containing ~200 μg Ca were dissolved in 3:1 (*v*/*v*) mixture of concentrated HF and HNO_3 in 6-mL Teflon beakers at 100 °C for three days. Then, the sample solutions were dried down and evaporated with 0.5 mL concentrated HCl at 120 °C twice. Finally, they were dissolved in 0.5 mL 2.5 N HCl. After dissolution, an aliquot of sample solution containing 30–50 μg Ca was mixed with an appropriate amount of ^{43}Ca-^{48}Ca double spike (Table S1), so that the ^{40}Ca/^{48}Ca in the mixture is ~8.7. Ca was separated using a cation exchange chromatography technique with AG50W-X12 Bio-Rad resin. Columns were precleaned and conditioned with 10 mL 6 N HCl, 5 mL MQ water, and 2 mL 2.5 N HCl. Samples were loaded using 50 μL 2.5 N HCl, and matrix elements were removed using 5 mL 2.5 N HCl. Finally, Ca was collected using 3.5 mL

Table 1
Stable Ca Isotopic Compositions From Kilauea, Hawaii

Sample ID	Weight (mg)	$\delta^{44/40}$Ca	2 SE	$\delta^{44/42}$Ca	2 SE	$\delta^{42/40}$Ca	2 SE	MgO (%)[a]	CaO (%)[a]	Sc (ppm)[b]	Sr/Nd[b]	n[c]
KI81-1-169.9	5.81	0.77	0.02	0.40	0.03	0.43	0.03	26.9	5.3	18.3	23.6	8
KI67–3-6.8	5.72	0.79	0.04	0.40	0.04	0.39	0.05	25.8	6.3	19.6	19.2	8
KI81–1-210.0	3.42	0.86	0.03	0.38	0.02	0.47	0.03	24.5	7.7	22.1	21.5	8
Iki-22	3.71	0.81	0.05	0.40	0.04	0.41	0.03	19.5	8.3	24.2	19.5	8
KI79–3-150.4	2.76	0.80	0.03	0.37	0.03	0.43	0.02	13.5	10.8	30.6	22.7	8
KI75–1-38.9	3.99	0.76	0.02	0.34	0.02	0.42	0.03	12.5	10.5	-	-	8
KI67–3-39.0	3.17	0.80	0.03	0.40	0.05	0.41	0.05	10.7	10.7	31.4	19.2	8
Iki-58	3.54	0.78	0.04	0.37	0.04	0.42	0.03	8.1	11.9	32.6	18.1	8
KI75–1-121.5	3.25	0.76	0.03	0.34	0.03	0.41	0.03	7.8	11.0	31.9	16.7	8
KI67–3-80.7	2.24	0.78	0.02	0.39	0.02	0.40	0.02	7.7	11.0	-	-	11
BHVO-2	2.90	0.80	0.03	0.37	0.01	0.42	0.03	7.2	11.4	32.0	15.6	7
BHVO-2 duplicate	2.97	0.80	0.04	0.36	0.04	0.44	0.02					11
BHVO-2 triplicate	4.61	0.84	0.03	0.39	0.03	0.45	0.02					12
BHVO-1	3.57	0.77	0.04	0.36	0.03	0.41	0.03	7.2	11.4	31.8	16.1	7
KI75–1-75.2	3.90	0.80	0.06	0.34	0.02	0.45	0.04	5.8	10.0	32.8	16.0	8
KI67–2-85.7	2.76	0.87	0.05	0.40	0.04	0.48	0.04	2.6	6.3	20.0	6.4	7
KI67–2-85.7 duplicate	4.26	0.87	0.06	0.40	0.03	0.47	0.05					8
KI81–2-88.6	2.63	0.74	0.04	0.36	0.03	0.38	0.05	2.4	6.1	18.8	6.1	7
Puna dacite	5.75	0.77	0.03	0.38	0.03	0.38	0.03	2.29	2.49	-	-	8
NIST SRM915a		0.01	0.02	0.01	0.02	0.00	0.02					38
Seawater		1.89	0.04	0.93	0.05	0.97	0.03					10

[a]Major element data from Murata and Richter (1966) and Helz et al. (1994), and Puna dacite from Teplow et al. (2009). [b]Trace element data from Helz (2012). [c]Number of repeat measurements by TIMS. Multiple measurements of each sample are reported in Table S4.

2.5 N HCl. All samples were passed through the column twice. The total Ca recovery after two column chemistry is ~90%. Because samples have been spiked before column chemistry, and the Ca isotopic fractionation on the columns also follows the exponential law (Zhu et al., 2016), the 90% recovery rate does not affect the measured Ca isotopic compositions (He et al., 2017). The total Ca blank was 10 ng, negligible compared to the 30–50 μg Ca used for each measurement. Ca isotopic analyses were performed on a Thermo-Finnigan Triton Plus TIMS using a double Re filament assembly. This instrument is equipped with two customized Faraday cups, L5 for ^{40}Ca and H4 for ^{48}Ca, allowing static measurement of masses from 40 to 48 amu. Purified Ca was loaded using 3% HNO_3, and measured with a total current of 100–300 pA and a ^{40}Ca signal between 8 and 30 V. Each collection contains 120 cycles, grouped in eight blocks. Data deduction was performed offline using an iterative method and the exponential fractionation law (Russell et al., 1978). Ca isotopic ratios are reported as δ values relative to NIST SRM 915a ($\delta^{4i/4j}Ca = [(^{4i}Ca/^{4j}Ca)_{sample}/(^{4i}Ca/^{4j}Ca)_{SRM915a} - 1] \times 1{,}000$). Each sample has been measured multiple times (usually 8 times), and the mean values and two standard errors are reported. Long-term reproducibilities at China University of Geosciences, Beijing, lab are about ±0.07 and ±0.03 for $\delta^{44/40}$Ca and $\delta^{44/42}$Ca, respectively, which are estimated based on multiple measurements of ten rock standards (He et al., 2017). Figure S2 shows the comparison of $\delta^{44/40}$Ca of standard samples measured in this lab (He et al., 2017) and the published values. The good agreement demonstrates the robustness of our analytical methods.

4. Results

Ca isotopic compositions of 16 Kilauea samples, including USGS standards BHVO-1, -2, and the Puna dacite, are reported in Table 1, and their individual measurements are in Table S4. The $\delta^{44/40}$Ca, $\delta^{44/42}$Ca, and $\delta^{42/40}$Ca values of our studied samples plot on the mass-dependent exponential fractionation lines (Figure 3), indicating insignificant accumulation of radiogenic ^{40}Ca. All measured Kilauea samples have homogeneous $\delta^{44/40}$Ca within uncertainty, ranging from 0.74 ± 0.04 to 0.87 ± 0.06 with a mean of 0.80 ± 0.08 (2 SD, n = 19, including duplicate measurements). There is no difference between Kilauea Iki samples and others from Kilauea (BHVO-1, -2, and the Puna dacite).

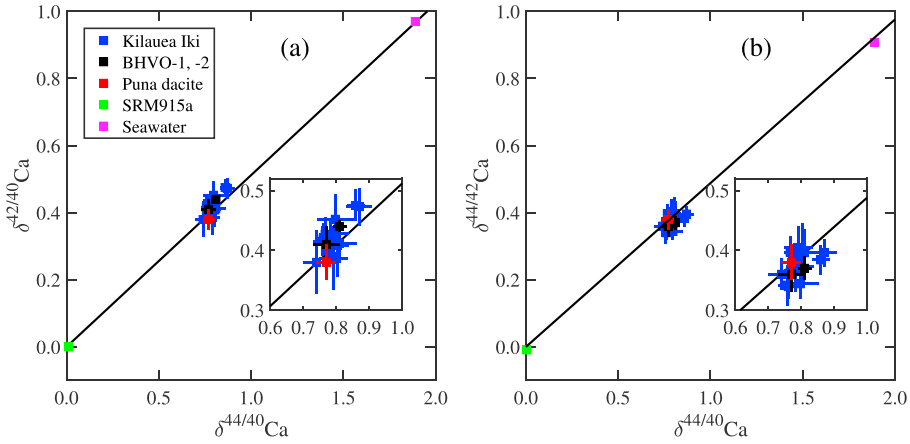

Figure 3. Ca three-isotope diagram of measured Kilauea samples together with seawater and NIST SRM915a. The exponential fractionation lines are calculated following Russell et al. (1978). Error bars represent 2 SE uncertainty. Kilauea samples are also shown in an inset in each panel.

5. Discussions

5.1. Crystal Fractionation History of Kilauea Iki Lava Lake Magma

In order to quantify the crystal fractionation history of Kilauea Iki lava lake basalts, we applied MELTS_Excel (Gualda & Ghiorso, 2015) to constrain their crystallization history. We used Iki-2 as the starting composition (sample S-4 of Murata & Richter, 1966). It is a sample from the 1959 summit eruption, which formed the Kilauea Iki lava lake (Murata & Richter, 1966), and has a MgO content of 11.50 wt % with ~8 wt % olivine. In our MELTS calculation, pressure was set at 1 bar, and the system was open to oxygen exchange at QFM buffer (Carmichael & Ghiorso, 1986). MELTS calculation shows that the liquidus temperature of the starting composition, Iki-2, is 1,282 °C. The temperature was then decreased at steps of 5 °C. Above 1,175 °C, olivine was the only crystal phase, and it was completely removed from the system in our model calculation. Below 1,175 °C, at a melt MgO of ~7.5 wt %, multiple phases (clinopyroxene, pigeonite, plagioclase, and oxides) crystallized. Starting from this point, the melt composition may not follow the observed trend of samples. In this case, part of the crystallized minerals was not removed, and was assumed to mix with the residual melt to fit the observed major element-major element trend. For samples with MgO higher than 11.50 wt %, the MgO content of Iki-2, $Fo_{86.5}$ olivine was added to model an olivine accumulation trend. Each step of crystallization was treated as an equilibrium crystallization process. However, the whole process of our model is close to a fractional crystallization process. We also monitored the trace element contents during our model calculation. Specifically, the abundances of a trace element of interest in the melts before and after each crystallization step are expressed as

$$C_2 = \frac{C_1}{f + \sum_{i=1}^{n} D_i * f_i} \quad (1)$$

in which C_1 and C_2 are the element contents of the melts before and after each crystallization step, respectively. f and f_i are the fractions of the melt and crystallizing mineral i, respectively. D_i is the mineral-melt partition coefficient of mineral i, given in Table S2 (Bennett et al., 2004; Elkins et al., 2008; Higuchi & Nagasawa, 1969; Horn et al., 1994; Keleman & Dunn, 1992; Klemme et al., 2006; Lemarchand et al., 1987; McKenzie & O'Nions, 1991; Nielsen et al., 1992; Paster et al., 1974; Sobolev et al., 1996).

Our model results are reported in Table S5, and shown in Figures 4 and S3, including CaO and Sc contents, Sr/Nd, and the proportions of removed minerals as functions of MgO content. As mentioned above, we forced the major element compositions of the magma + residual minerals to follow the observed Kilauea Iki trend. The good agreement between the modeled trace element contents (Sc and Sr/Nd) of the magma + residual minerals and those observed in Kilauea Iki basalts validates our approach (Figure 4).

The evolution of the CaO content Kilauea Iki lavas can be divided into two stages. In the first stage, CaO content increases with decreasing MgO due to olivine crystallization and accumulation. In the second stage, CaO and Sc contents and Sr/Nd decrease with decreasing MgO content as a consequence of crystallization of

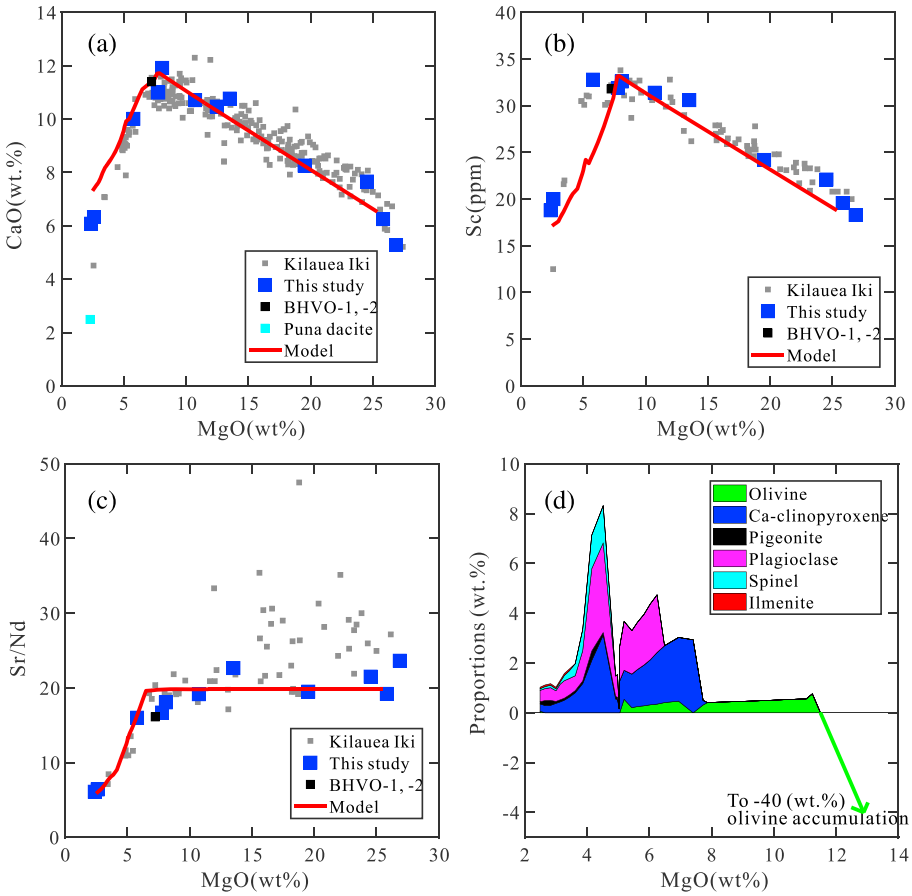

Figure 4. (a) CaO content (%), (b) Sc concentration (ppm), and (c) Sr/Nd versus MgO content (%) for Kilauea Iki lava lake samples (Helz, 2012; Helz et al., 1994; Helz & Taggart, 2010; Murata & Richter, 1966), Puna dacite, and BHVO-1, -2. Red line shows our modeled MELTS calculation result for crystal fractionation of Iki-2 at oxygen fugacity buffered at QFM and 1 bar (Table S5). Blue squares represent the Kilauea Iki lava lake samples used in this study, and gray squares are other Kilauea Iki lava lake samples. (d) Area plot for weight proportions of crystallized minerals removed from the system as a function of MgO content during magma evolution. Green line shows the olivine accumulation trend.

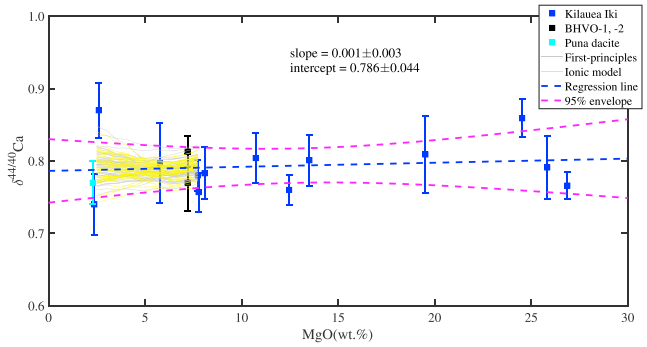

Figure 5. MgO (%) versus $\delta^{44/40}$Ca for Kilauea lavas. Regression line (blue dashed line) with the 95% C.I. envelope (pink dashed lines) of measured Kilauea Iki lavas are shown. The pale colored lines are MgO-$\delta^{44/40}$Ca evolution model lines from our Monte Carlo simulations. Pale gray lines were calculated using intermineral Ca isotopic fractionation factors from first-principles calculations, and pale yellow lines the ionic model results. See section 5.2 for details.

Ca-rich clinopyroxene and plagioclase. This crystallized phase assemblage was observed in Kilauea Iki lavas (Pitcher et al. 2009, Figures 6 and 7).

5.2. Mineral-Melt Ca Isotopic Fractionation Factor Inferred From the Lack of Ca Isotopic Fractionation During Basaltic Magma Differentiation

The overall horizontal MgO-$\delta^{44/40}$Ca trend of Kilauea Iki lavas implies that Ca isotopic fractionation is insignificant during basalt magmatic differentiation at current analytical precision (±0.07 for $\delta^{44/40}$Ca). We use the MgO-$\delta^{44/40}$Ca trend of Kilauea lavas (Figure 5) to constrain the Ca isotopic fractionation factors between minerals and basaltic melt. Similar to the trace element effects discussed in section 5.1, the melt Ca isotopic compositions before and after each crystallization step can be expressed as

$$\delta^{44/40}Ca^{melt,1} = \frac{\delta^{44/40}Ca^{melt,2}\times f_{melt,2}\times CaO^{melt,2} + \sum_{i=1}^{3}\delta^{44/40}Ca^{i}\times f_{i,2}\times CaO^{i,2}}{f_{melt,2}\times CaO^{melt,2} + \sum_{i=1}^{3} f_{i,2}\times CaO^{i,2}} \quad (2)$$

$$\delta^{44/40}Ca^{i} = \Delta^{44/40}Ca^{i-melt} + \delta^{44/40}Ca^{melt,2} \quad (3)$$

$\delta^{44/40}Ca^{melt,1}$ and $\delta^{44/40}Ca^{melt,2}$ are the Ca isotopic compositions of the melts before and after crystallization, respectively. $\delta^{44/40}Ca^{i}$ is the Ca

Table 2
Parameters for $10^3 ln\beta$ of $^{44}Ca/^{40}Ca$ From First-Principles Calculations

Minerals	Formula	Ca–O bond length (Å)	Coordination number	*a*
Clinopyroxene[a]	$Ca_{15/32}Mg_{17/32}SiO_3$	2.469	8	1.50
Plagioclase[b]	$CaAl_2Si_2O_8$	2.580	8	1.31
Pigeonite[b]	$Ca_{1/8}Mg_{7/8}SiO_3$	2.375	7	1.92
Orthopyroxene[a]	$Ca_{1/32}Fe_{3/32}Mg_{7/8}SiO_3$	2.326	6	1.92

Note. $10^3 ln^{44/40}\beta = a/(T/1{,}000)^2$, where *T* is the temperature in kelvin. We ignored the high-order terms because of their insignificant contributions. Clinopyroxene, plagioclase, and pigeonite are used in model calculations of crystal fractionation of Kilauea Iki lava lake samples. Clinopyroxene and orthopyroxene are used in model calculations of partial melting of the mantle.
[a]Data source from Wang et al. (2017). [b]Data source from Zhou et al. (2016).

isotopic composition of mineral *i*. $f_{melt,2}$ and $f_{i,2}$ are the fractions of melt and crystallized mineral *i*, respectively, after crystallization. $CaO^{melt,2}$ and $CaO^{i,2}$ are the CaO contents of melt and crystallized mineral *i*, respectively, after crystallization. Three Ca-bearing minerals, clinopyroxene, pigeonite, and plagioclase, are involved during magma evolution at Kilauea Iki (Figure 4d and Table S5). The Ca isotopic fractionation between clinopyroxene and melt is expressed as

$$\Delta^{44/40}Ca^{cpx-melt} = \frac{a}{(T/1000)^2} \quad (4)$$

and other mineral-melt fractionation factors can be expressed as

$$\Delta^{44/40}Ca^{pgt-melt} = \Delta^{44/40}Ca^{pgt-cpx} + \Delta^{44/40}Ca^{cpx-melt} \quad (5)$$

$$\Delta^{44/40}Ca^{pl-melt} = \Delta^{44/40}Ca^{pl-cpx} + \Delta^{44/40}Ca^{cpx-melt} \quad (6)$$

The intermineral Ca isotopic fractionation factors can be calculated independently (see below), so that the only unknown parameter is the coefficient *a* in equation (4). In the following sections, we will solve equation-(2) to constrain this coefficient using available intermineral Ca isotopic fractionation factors, which are primarily controlled by their Ca-O bond length difference, Ca coordination numbers, and temperature (Feng et al., 2014; Huang et al., 2010; Wang et al., 2017; Young et al., 2015). In this study, two sets of intermineral Ca isotopic fractionation factors are used, one obtained by first-principles calculations (Wang et al., 2017; Zhou et al., 2016) and the other by the ionic model presented in Young et al. (2015).

5.2.1. Intermineral Fractionation Factors Constrained by First-Principles Calculations

The Ca isotopic fractionation factors between clinopyroxene-plagioclase and clinopyroxene-pigeonite can be obtained using the reduced partition function ratios by first-principles calculations (Wang et al., 2017; Zhou et al., 2016) summarized in Table 2. Using equations (2)–(6), the above specified intermineral Ca isotopic fractionation factors (Table 2), and the crystallized mineral assemblage (section 5.1), the MgO-$\delta^{44/40}Ca$ trend of Kilauea Iki lavas can be used to estimate $\Delta^{44/40}Ca^{cpx\text{-}melt}$. A Monte Carlo approach was used. We used the $\delta^{44/40}Ca$ values on the 95% C.I. envelope at MgO = 11.5 wt % ($\delta^{44/40}Ca$ = 0.79 ± 0.02, 2 SD) and MgO = 3 wt % ($\delta^{44/40}Ca$ = 0.79 ± 0.04, 2 SD) as our starting and final values, respectively. Fifty groups of normally distributed starting and final $\delta^{44/40}Ca$ values were randomly generated. In each simulation, 10,000 normally distributed $\Delta^{44/40}Ca^{pl\text{-}cpx}$ and $\Delta^{44/40}Ca^{pgt\text{-}cpx}$ values were randomly produced with a relative uncertainty of 7%, typical of the uncertainty from first-principles calculations (Kowalski et al., 2013; Méheut et al., 2009).

The estimated mineral-melt Ca fractionation factors are summarized in Table 3. To the best of our knowledge, they are the first mineral-melt Ca isotopic fractionation factors inferred based on measurements of natural basalts.

5.2.2. Intermineral Fractionation Factors Constrained by an Ionic Model

Under the ionic model described by Young et al. (2015), the intermineral Ca isotopic fractionation is expressed as

Table 3
Estimated Mineral-Melt Ca Fractionation Factors

Minerals	Formula	*a*					
		First principles	2 SD	Ionic model	2 SD	Average	2 SD
Clinopyroxene	$Ca_{15/32}Mg_{17/32}SiO_3$	0.07	0.05	0.11	0.05	0.09	0.07
Plagioclase	$CaAl_2Si_2O_8$	−0.12	0.06	−0.17	0.07	−0.15	0.08
Pigeonite	$Ca_{1/8}Mg_{7/8}SiO_3$	0.49	0.08	0.39	0.07	0.44	0.13
Orthopyroxene	$Ca_{1/32}Fe_{3/32}Mg_{7/8}SiO_3$	0.49	0.08	0.55	0.08	0.52	0.10

$\Delta^{44/40}Ca^{mineral\text{-}melt} = a/(T/1{,}000)^2$, where *T* is the temperature in kelvin.

$$\Delta^{44/40}Ca^{A-B} = \frac{1000}{24}\left(\frac{h}{k_bT}\right)^2\left(\frac{1}{m_{40}}-\frac{1}{m_{44}}\right)\left(\frac{K_{f,A}}{4\pi^2}-\frac{K_{f,B}}{4\pi^2}\right) \quad (7)$$

where m_{40} and m_{44} are the atomic masses of ^{40}Ca and ^{44}Ca, respectively; k_b is the Boltzmann's constant ($1.3806503 \times 10^{-23}$ $m^2{\cdot}kg/s^2{\cdot}K$); h is the Planck's constant (6.626068×10^{-34} $m^2{\cdot}kg/s$); T is the temperature in kelvin; and $K_{f,j}$ is treated as electrostatic in origin and expressed as

$$K_{f,j} = \frac{z_{Ca}z_O e^2(1-n)}{4\pi\varepsilon_0 r_{Ca-O}^3} \quad (8)$$

where ε_0 is the electric constant ($8.85418782 \times 10^{-12}$ $s^4{\cdot}A^2/m^3{\cdot}kg$), e is the charge of an electron ($1.60217646 \times 10^{-19}$ C), $r_{Ca\text{-}O}$ is the mean Ca-O bond length, n is the exponent in the Born–Mayer formulation for ion repulsion ($n = 12$), and z_i is the effective charge of the ion. Using the Ca-O bond lengths summarized in Table 2, we have

$$\Delta^{44/40}Ca^{pl-cpx} = -\frac{0.28}{(T/1000)^2} \quad (9)$$

$$\Delta^{44/40}Ca^{pgt-cpx} = \frac{0.28}{(T/1000)^2} \quad (10)$$

Using the Monte Carlo approach described in section 5.2.1, we also estimated the mineral-melt Ca isotopic fractionation factors, which are reported in Table 3. The mineral-melt Ca isotopic fractionation factors obtained using two approaches agree within errors, and the averages are reported in Table 3. Specifically, the clinopyroxene-melt Ca isotopic fractionation factor is:

$$\Delta^{44/40}Ca^{cpx-melt} = \frac{0.09\pm0.07}{(T/1000)^2} \quad (11)$$

At 1,200 °C, $\Delta^{44/40}Ca^{cpx\text{-}melt} = 0.04 \pm 0.03$. That is, at magmatic temperature, the Ca isotopic fractionation between basaltic melt and clinopyroxene is very small.

5.3. Implication for Ca Isotopic Fractionation During Peridotite Partial Melting Under 1–2 GPa

Based on the inferred mineral-melt Ca isotopic fractionation factors (section 5.2 and Table 3), as well as additional mineral-mineral Ca isotopic fractionation factors (Wang et al., 2017), we explored Ca isotopic fractionation during partial melting of spinel peridotite. We restricted our exercise to low pressure at 1–2 GPa, because both the mineral and melt structures are sensitive to pressure (e.g., Bajgain et al., 2015; Huang et al., 2014; Wu et al., 2015), and it is unclear whether our inferred mineral-melt Ca isotopic fractionation factors in section 5.2 can be directly applied to high pressure within the garnet stability field.

In order to explore the Ca isotopic effects during different types of partial melting, we have run the following simulations: batch, fractional, and dynamic melting of the primitive mantle (McDonough & Sun, 1995) under 2 GPa. We also ran simulations of batch melting of the depleted MORB mantle (Workman & Hart, 2005) and West Kettle River spinel lherzolite xenolith (Walter, 1998) under 2 GPa to explore possible compositional effects on Ca isotopes. Finally, we ran simulations of batch melting of the primitive mantle under 1 GPa to explore possible pressure effects.

We used the pMELTS program (Ghiorso et al., 2002) to model the fractions and compositions of the melt and coexisting minerals during batch partial melting at low pressure (1–2 GPa). The degree of partial melting ranged from ~5 to ~30%. Oxygen fugacity buffer was set at QFM. The fractions and compositions of the melts and their coexisting minerals are reported in Table S6. $\delta^{44/40}$Ca in batch melt was obtained using mass balance relationship, and are reported in Tables S7 and S8:

$$\delta^{44/40}Ca^0 = \frac{\delta^{44/40}Ca^{melt}\times F_{melt}\times CaO^{melt} + \sum_{i=1}^{N}\delta^{44/40}Ca^i\times F_i\times CaO^i}{F_{melt}\times CaO^{melt} + \sum_{i=1}^{N}F_i\times CaO^i} \quad (12)$$

where $\delta^{44/40}Ca^0$ is the mantle Ca isotopic composition (+0.94; Kang et al., 2017). Superscript *melt* and *i* refer to melt and mineral *i*, respectively. *F* is the fraction of the melt, and F_i is the fraction of mineral *i*. CaO represents

the concentration (wt %). *N* is the number of total coexisting minerals. The Ca isotopic composition of bulk residue is calculated as the weighted average of the mineral Ca isotopic compositions (Tables S7 and S8).

We also explored another two partial melting scenarios using primitive mantle as the starting composition under 2 GPa: a fractional melting and a dynamic melting in which 5% melt is trapped with residues. The fractions and compositions of melts and coexisting minerals are reported in Table S6, and their $\delta^{44/40}$Ca are reported in Tables S7 and S8.

Mantle clinopyroxenes have different compositions compared to those fractionated from Kilauea Iki basalts. Mantle clinopyroxenes have CaO of 12–17 wt %, and those fractionated from Kilauea Iki basalts have CaO of 17–20 wt %. This reflects a temperature effect on pyroxene compositions. Kilauea Iki lava lake magma evolved below 1,300 °C, while mantle partial melting occurs above 1,300 °C. Under higher temperatures, orthopyroxene becomes more Ca-rich and clinopyroxene less Ca-rich (e.g., Nickel & Brey, 1984). Wang et al. (2017) reported Ca concentration effect on the reduced partition function ratio of Ca isotopes of clinopyroxene, 1,000 $\ln^{44/40}\beta_{cpx}$. When Ca/(Ca + Mg + Fe) is less than 0.5, all Ca atoms occupy the larger eightfold coordinated M2 sites. When Ca/(Ca + Mg + Fe) is greater than 0.5, some Ca atoms have to occupy the smaller sixfold coordinated M1 sites. As a consequence, this leads to variable Ca-O bond length and 1,000 $\ln^{44/40}\beta_{cpx}$ (Wang et al., 2017). However, the temperatures associated with mantle melting are above 1,300 °C in our simulations (Table S6). Under such high temperatures, the Ca concentration effect on 1,000 $\ln^{44/40}\beta_{cpx}$ is less than 0.03 (Wang et al. 2017, Figure 6). This concentration effect on $\delta^{44/40}$Ca in calculated melts and residues is less than 0.02. Consequently, it is ignored in our simulations.

We simulated Ca isotopic effects during mantle partial melting using mineral-melt fractionation factors obtained by two approaches, which agree within uncertainty (Table 3). The simulated Ca isotopic effects in melts and residues are in Table S7 (for first-principles calculations) and Table S8 (for the ionic model). Since both results agree within uncertainty, we only plot the results from the first-principles calculations (Table S7) in Figure 1, in which they are compared to natural rocks. The important observations include the following:

1. There is negligible effect on the melt $\delta^{44/40}$Ca because most Ca budget is in the melt. In detail, melt $\delta^{44/40}$Ca ranges from 0.89 to 0.93 in all our simulations, including three types of starting materials (primitive and depleted mantle) under 1 and 2 GPa, and three types of partial melting. These values are indistinguishable from the mantle value of 0.94 used in our simulation. Hence, the observed low $\delta^{44/40}$Ca in N-MORB from southern Juan de Fuca ridge (Zhu et al., 2018) may not reflect a partial melting effect.
2. Large $\delta^{44/40}$Ca effects are observed in melting residues. This may explain the heavy Ca isotopic compositions reported in dunites and some peridotites (Amini et al., 2009; Feng et al., 2017; Huang et al., 2010). However, caution must be exercised when applying our results to explain the Ca isotopic compositions in dunites, because many dunites have been described as melt channels instead of large degree partial melting residues (e.g., Kelemen et al., 1992). $\delta^{44/40}$Ca of residues are not sensitive to starting materials or melting pressure, but to partial melting styles. Specifically,

(a) the maximum $\delta^{44/40}$Ca of residues in batch melting is ~1.1. This basically reflects the Ca isotopic fractionation between orthopyroxene and melt, because at large degrees of batch melting, orthopyroxene is the only Ca-bearing mineral in the residues.
(b) The $\delta^{44/40}$Ca of residues in fractional melting can reach up to 1.25 at a partial melting degree of 30%, and it will increase further with increasing melting degree.
(c) The $\delta^{44/40}$Ca versus MgO relationship of residues in dynamic melting mimics that of the fractional melting, but the $\delta^{44/40}$Ca effects are smaller because of the trapped melt. Specifically, at 30% partial melting, residue of dynamic melting has $\delta^{44/40}$Ca of 1.12, compared to 1.25 in fractional melting.

3. Overall, our simulations show that partial melting under 1–2 GPa can produce up to 0.3 $\delta^{44/40}$Ca variation in melts and residues.

6. Conclusions

1. There is no measurable $^{44}Ca/^{40}Ca$ variation (at a level of ±0.07‰) in Kilauea basalts, although some have undergone significant fractionation of Ca-rich minerals, including up to 30% clinopyroxene, 28% plagioclase, and 1.7% pigeonite.

2. Based on the lack of Ca isotopic fractionation during basaltic evolution, the clinopyroxene-melt Ca isotopic fractionation factor is estimated at $(0.09 \pm 0.07)/(T/1{,}000)^2$ (T in kelvin). To the best of our knowledge, this is the first estimated mineral-basalt Ca isotopic fractionation factor based on measurements of natural basalts.
3. Our model simulations show that mantle partial melting under 1–2 GPa may result in no detectable $\delta^{44/40}$Ca isotopic fractionation (<0.07) in melts. Residues produced by fractional and dynamic melting are characterized by heavier Ca isotopes, with $\delta^{44/40}$Ca up to +0.3 higher than their source value.
4. Our model calculations predict negligible Ca isotopic fractionation in melts during crystal fractionation of tholeiitic magmas and partial melting of spinel peridotite. Consequently, the observed Ca isotopic variation in basalts ($\delta^{44/40}$Ca = 0.59–1.36; Figure 1) most likely reflects source heterogeneity.

Acknowledgments
This work was supported by the National Nature Science Foundation of China (41673012, 41230209, and 41473003), and National Science Foundation (EAR1144727 and EAR1524387). Y.S.H. and S.H. also acknowledge support from the State Key Laboratory of Geological Processes and Mineral Resources (Open Research Program GPMR201510). We thank Chen Zhou and Zhongqing Wu for discussions and Vincent Salters, Paolo Sossi, Justin Simon, and an anonymous reviewer for their critical, but constructive comments, which significantly improved the manuscript. Finally, we thank Janne Blichert-Toft for handling our submission. Isotopic data are presented in the main text. Multiple measurements of each sample and model data of MELTS_excel and pMELTS are reported in the supporting information.

References

Amini, M., Eisenhauer, A., Böhm, F., Holmden, C., Kreissig, K., Hauff, F., & Jochum, K. P. (2009). Calcium isotopes ($\delta^{44/40}$Ca) in MPI-DING reference glasses, USGS rock powders and various rocks: Evidence for Ca isotope fractionation in terrestrial silicates. *Geostandards and Geoanalytical Research*, *33*(2), 231–247. https://doi.org/10.1111/j.1751-908X.2009.00903.x

Bajgain, S., Ghosh, D. B., & Karki, B. B. (2015). Structure and density of basaltic melts at mantle conditions from first-principles simulations. *Nature Communications*, *6*(1), 8578. https://doi.org/10.1038/ncomms9578

Bennett, S. L., Blundy, J., & Elliott, T. (2004). The effect of sodium and titanium on crystal-melt partitioning of trace elements. *Geochimica et Cosmochimica Acta*, *68*(10), 2335–2347. https://doi.org/10.1016/j.gca.2003.11.006

Carmichael, I. S. E., & Ghiorso, M. S. (1986). Oxidation-reduction relations in basic magma: A case for homogeneous equilibria. *Earth and Planetary Science Letters*, *78*(2–3), 200–210. https://doi.org/10.1016/0012-821X(86)90061-0

Chen, H., Savage, P. S., Teng, F.-Z., Helz, R. T., & Moynier, F. (2013). Zinc isotope fractionation during magmatic differentiation and the isotopic composition of the bulk earth. *Earth and Planetary Science Letters*, *369-370*, 34–42. https://doi.org/10.1016/j.epsl.2013.02.037

Colla, C. A., Wimpenny, J., Yin, Q.-Z., Rustad, J. R., & Casey, W. H. (2013). Calcium-isotope fractionation between solution and solids with six, seven or eight oxygens bound to Ca(II). *Geochimica et Cosmochimica Acta*, *121*, 363–373. https://doi.org/10.1016/j.gca.2013.07.041

Coplen, T. B., Böhlke, J. K., De Bièvre, P., Ding, T., Holden, N. E., Hopple, J. A., et al. (2002). Isotope-abundance variations of selected elements (IUPAC technical report). *Pure and Applied Chemistry*, *74*(10), 1987–2017. https://doi.org/10.1351/pac200274101987

DePaolo, D. J. (2004). Calcium isotopic variations produced by biological, kinetic, radiogenic and nucleosynthetic processes. *Reviews in Mineralogy and Geochemistry*, *55*(1), 255–288. https://doi.org/10.2138/gsrmg.55.1.255

Elkins, L. J., Gaetani, G. A., & Sims, K. W. W. (2008). Partitioning of U and Th during garnet pyroxenite partial melting: Constraints on the source of alkaline ocean island basalts. *Earth and Planetary Science Letters*, *265*(1–2), 270–286. https://doi.org/10.1016/j.epsl.2007.10.034

Fantle, M. S., & Tipper, E. T. (2014). Calcium isotopes in the global biogeochemical Ca cycle: Implications for development of a Ca isotope proxy. *Earth-Science Reviews*, *129*, 148–177. https://doi.org/10.1016/j.earscirev.2013.10.004

Feng, C., Qin, T., Huang, S., Wu, Z., & Huang, F. (2014). First-principles investigations of equilibrium calcium isotope fractionation between clinopyroxene and ca-doped orthopyroxene. *Geochimica et Cosmochimica Acta*, *143*, 132–142. https://doi.org/10.1016/j.gca.2014.06.002

Feng, L.-p., Zhou, L., Yang, L., DePaolo, D. J., Tong, S.-Y., Liu, Y.-S., et al. (2017). Calcium isotopic compositions of sixteen USGS reference materials. *Geostandards and Geoanalytical Research*, *41*(1), 93–106. https://doi.org/10.1111/ggr.12131

Ghiorso, M. S., Hirschmann, M. M., Reiners, P. W., & Kress, V. C. (2002). The pMELTS: A revision of MELTS for improved calculation of phase relations and major element partitioning related to partial melting of the mantle to 3 GPa. *Geochemistry, Geophysics, Geosystems*, *3*(5), 1030. https://doi.org/10.1029/2001GC000217

Greaney, A. T., Rudnick, R. L., Helz, R. T., Gaschnig, R. M., Piccoli, P. M., & Ash, R. D. (2017). The behavior of chalcophile elements during magmatic differentiation as observed in Kilauea Iki lava lake, Hawaii. *Geochimica et Cosmochimica Acta*, *210*, 71–96. https://doi.org/10.1016/j.gca.2017.04.033

Gualda, G. A. R., & Ghiorso, M. S. (2015). MELTS_excel: A Microsoft Excel-based MELTS interface for research and teaching of magma properties and evolution. *Geochemistry, Geophysics, Geosystems*, *16*, 315–324. https://doi.org/10.1002/2014GC005545

He, Y., Wang, Y., Zhu, C., Huang, S., & Li, S. (2017). Mass-independent and mass-dependent Ca isotopic compositions of thirteen geological reference materials measured by thermal ionisation mass spectrometry. *Geostandards and Geoanalytical Research*, *41*(2), 283–302. https://doi.org/10.1111/ggr.12153

Helz, R. T. (1987). Differentiation behaviour of Kilauea Iki lava lake, Kilauea volcano, Hawaii: An overview of past and current work. In B. O. Mysen (Ed.), *Magmatic Processes: Physiochemical Principles* (pp. 241–258). St. Louis: Geochemical Society.

Helz, R. T. (2012). Trace-element analyses of core samples from the 1967–1988 drillings of Kilauea Iki lava Lake, Hawaii. *U.S.* Geological Survey Open File Report, 2012-1050, 1–56.

Helz, R. T., Kirschenbaum, H., Marinenko, J. W., & Qian, R. (1994). Whole rock analyses of core samples from the 1967, 1975, 1979 and 1981 drillings of Kilauea Iki lava lake, Hawaii. *U.S.* Geological Survey Open File Report, 94-684, 1–65.

Helz, R. T., & Taggart, J. E. Jr. (2010). Whole-rock analyses of core samples from the 1988 drilling of Kilauea Iki lava lake, Hawaii. *U.S.* Geological Survey Open File Report, 2010-1093, 1–47.

Helz, R. T., & Thornber, C. R. (1987). Geothermometry of Kilauea Iki lava lake, Hawaii. *Bulletin of Volcanology*, *49*(5), 651–668. https://doi.org/10.1007/bf01080357

Higuchi, H., & Nagasawa, H. (1969). Partition of trace elements between rock-forming minerals and the host volcanic rocks. *Earth and Planetary Science Letters*, *7*(3), 281–287. https://doi.org/10.1016/0012-821X(69)90066-1

Holmden, C., & Bélanger, N. (2010). Ca isotope cycling in a forested ecosystem. *Geochimica et Cosmochimica Acta*, *74*(3), 995–1015. https://doi.org/10.1016/j.gca.2009.10.020

Horn, I., Foley, S. F., Jackson, S. E., & Jenner, G. A. (1994). Experimentally determined partitioning of high field strength- and selected transition elements between spinel and basaltic melt. *Chemical Geology*, *117*(1–4), 193–218. https://doi.org/10.1016/0009-2541(94)90128-7

Huang, F., Wu, Z., Huang, S., & Wu, F. (2014). First-principles calculations of equilibrium silicon isotope fractionation among mantle minerals. *Geochimica et Cosmochimica Acta*, *140*, 509–520. https://doi.org/10.1016/j.gca.2014.05.035

Huang, S., Farkaš, J., & Jacobsen, S. B. (2010). Calcium isotopic fractionation between clinopyroxene and orthopyroxene from mantle peridotites. *Earth and Planetary Science Letters*, *292*(3–4), 337–344. https://doi.org/10.1016/j.epsl.2010.01.042

Huang, S., Farkaš, J., & Jacobsen, S. B. (2011). Stable calcium isotopic compositions of Hawaiian shield lavas: Evidence for recycling of ancient marine carbonates into the mantle. *Geochimica et Cosmochimica Acta*, *75*(17), 4987–4997. https://doi.org/10.1016/j.gca.2011.06.010

Jacobson, A. D., Grace Andrews, M., Lehn, G. O., & Holmden, C. (2015). Silicate versus carbonate weathering in Iceland: New insights from Ca isotopes. *Earth and Planetary Science Letters*, *416*, 132–142. https://doi.org/10.1016/j.epsl.2015.01.030

Jochum, K. P., Stoll, B., Herwig, K., Willbold, M., Hofmann, A. W., Amini, M., et al. (2006). MPI-DING reference glasses for in situ microanalysis: New reference values for element concentrations and isotope ratios. *Geochemistry, Geophysics, Geosystems*, *7*, Q02008. https://doi.org/10.1029/2005GC001060

John, T., Gussone, N., Podladchikov, Y. Y., Bebout, G. E., Dohmen, R., Halama, R., et al. (2012). Volcanic arcs fed by rapid pulsed fluid flow through subducting slabs. *Nature Geoscience*, *5*(7), 489–492. https://doi.org/10.1038/ngeo1482

Kang, J.-T., Ionov, D. A., Liu, F., Zhang, C.-L., Golovin, A. V., Qin, L.-P., et al. (2017). Calcium isotopic fractionation in mantle peridotites by melting and metasomatism and Ca isotope composition of the bulk silicate earth. *Earth and Planetary Science Letters*, *474*, 128–137. https://doi.org/10.1016/j.epsl.2017.05.035

Kang, J.-T., Zhu, H.-L., Liu, Y.-F., Liu, F., Wu, F., Hao, Y.-T., et al. (2016). Calcium isotopic composition of mantle xenoliths and minerals from eastern China. *Geochimica et Cosmochimica Acta*, *174*, 335–344. https://doi.org/10.1016/j.gca.2015.11.039

Kato, C., Moynier, F., Foriel, J., Teng, F.-Z., & Puchtel, I. S. (2017). The gallium isotopic composition of the bulk silicate earth. *Chemical Geology*, *448*, 164–172. https://doi.org/10.1016/j.chemgeo.2016.11.020

Keleman, P. B., & Dunn, J. T. (1992). Depletion of Nb relative to other highly incompatible elements by melt/rock reaction in the upper mantle. *Eos, Transactions of the American Geophysical Union*, *73*, 656–657.

Kelemen, P. B., Dick, H. J. B., & Quick, J. E. (1992). Formation of harzburgite by pervasive melt/rock reaction in the upper mantle. *Nature*, *358*(6388), 635–641. https://doi.org/10.1038/358635a0

Klemme, S., Günther, D., Hametner, K., Prowatke, S., & Zack, T. (2006). The partitioning of trace elements between ilmenite, ulvospinel, armalcolite and silicate melts with implications for the early differentiation of the moon. *Chemical Geology*, *234*(3–4), 251–263. https://doi.org/10.1016/j.chemgeo.2006.05.005

Kowalski, P. M., Wunder, B., & Jahn, S. (2013). Ab initio prediction of equilibrium boron isotope fractionation between minerals and aqueous fluids at high P and T. *Geochimica et Cosmochimica Acta*, *101*, 285–301. https://doi.org/10.1016/j.gca.2012.10.007

Lehn, G. O., & Jacobson, A. D. (2015). Optimization of a ^{48}Ca–^{43}Ca double-spike MC-TIMS method for measuring Ca isotope ratios ($\delta^{44/40}$Ca and $\delta^{44/42}$Ca): Limitations from filament reservoir mixing. *Journal of Analytical Atomic Spectrometry*, *30*(7), 1571–1581. https://doi.org/10.1039/C4JA00412D

Lemarchand, F., Villemant, B., & Calas, G. (1987). Trace element distribution coefficients in alkaline series. *Geochimica et Cosmochimica Acta*, *51*(5), 1071–1081. https://doi.org/10.1016/0016-7037(87)90201-8

Liu, F., Li, X., Wang, G., Liu, Y., Zhu, H., Kang, J., et al. (2017). Marine carbonate component in the mantle beneath the southeastern Tibetan Plateau: Evidence from magnesium and calcium isotopes. *Journal of Geophysical Research: Solid Earth*, *122*, 9729–9744. https://doi.org/10.1002/2017JB014206

Liu, F., Zhu, H. L., Li, X., Wang, G. Q., & Zhang, Z. F. (2017). Calcium isotopic fractionation and compositions of geochemical reference materials. *Geostandards and Geoanalytical Research*, *41*, 675–688. https://doi.org/10.1111/ggr.12172

Magna, T., Gussone, N., & Mezger, K. (2015). The calcium isotope systematics of Mars. *Earth and Planetary Science Letters*, *430*, 86–94. https://doi.org/10.1016/j.epsl.2015.08.016

McDonough, W. F., & Sun, S. s. (1995). The composition of the earth. *Chemical Geology*, *120*(3–4), 223–253. https://doi.org/10.1016/0009-2541(94)00140-4

McKenzie, D., & O'Nions, R. K. (1991). Partial melt distributions from inversion of rare earth element concentrations. *Journal of Petrology*, *32*(5), 1021–1091. https://doi.org/10.1093/petrology/32.5.1021

Méheut, M., Lazzeri, M., Balan, E., & Mauri, F. (2009). Structural control over equilibrium silicon and oxygen isotopic fractionation: A first-principles density-functional theory study. *Chemical Geology*, *258*(1–2), 28–37. https://doi.org/10.1016/j.chemgeo.2008.06.051

Murata, K. J., & Richter, D. H. (1966). Chemistry of the lavas of the 1959–60 eruption of Kilauea volcano, Hawaii. *U.S.* Geological Survey Professional Paper, 537-A, 1–26.

Nickel, K. G., & Brey, G. (1984). Subsolidus orthopyroxene-clinopyroxene systematics in the system CaO-MgO-SiO_2 to 60 kb: A re-evaluation of the regular solution model. *Contributions to Mineralogy and Petrology*, *87*(1), 35–42. https://doi.org/10.1007/BF00371400

Nielsen, R. L., Gallahan, W. E., & Newberger, F. (1992). Experimentally determined mineral-melt partition coefficients for Sc, Y and REE for olivine, orthopyroxene, pigeonite, magnetite and ilmenite. *Contributions to Mineralogy and Petrology*, *110*(4), 488–499. https://doi.org/10.1007/BF00344083

Paster, T. P., Schauwecker, D. S., & Haskin, L. A. (1974). The behavior of some trace elements during solidification of the Skaergaard layered series. *Geochimica et Cosmochimica Acta*, *38*(10), 1549–1577. https://doi.org/10.1016/0016-7037(74)90174-4

Pitcher, L., Helz, R. T., Walker, R. J., & Piccoli, P. (2009). Fractionation of the platinum-group elements and re during crystallization of basalt in Kilauea Iki lava Lake, Hawaii. *Chemical Geology*, *260*(3–4), 196–210. https://doi.org/10.1016/j.chemgeo.2008.12.022

Richter, F. M., Davis, A. M., DePaolo, D. J., & Watson, E. B. (2003). Isotope fractionation by chemical diffusion between molten basalt and rhyolite. *Geochimica et Cosmochimica Acta*, *67*(20), 3905–3923. https://doi.org/10.1016/S0016-7037(03)00174-1

Russell, W. A., Papanastassiou, D. A., & Tombrello, T. A. (1978). Ca isotope fractionation on the earth and other solar system materials. *Geochimica et Cosmochimica Acta*, *42*(8), 1075–1090. https://doi.org/10.1016/0016-7037(78)90105-9

Ryu, J.-S., Jacobson, A. D., Holmden, C., Lundstrom, C., & Zhang, Z. (2011). The major ion, $\delta^{44/40}$Ca, $\delta^{44/42}$Ca, and $\delta^{26/24}$Mg geochemistry of granite weathering at pH = 1 and T = 25 °C: Power-law processes and the relative reactivity of minerals. *Geochimica et Cosmochimica Acta*, *75*(20), 6004–6026. https://doi.org/10.1016/j.gca.2011.07.025

Schiller, M., Paton, C., & Bizzarro, M. (2012). Calcium isotope measurement by combined HR-MC-ICPMS and TIMS. *Journal of Analytical Atomic Spectrometry*, *27*(1), 38–49. https://doi.org/10.1039/C1JA10272A

Simon, J. I., & DePaolo, D. J. (2010). Stable calcium isotopic composition of meteorites and rocky planets. *Earth and Planetary Science Letters*, *289*(3–4), 457–466. https://doi.org/10.1016/j.epsl.2009.11.035

Simon, J. I., Jordan, M. K., Tappa, M. J., Schauble, E. A., Kohl, I. E., & Young, E. D. (2017). Calcium and titanium isotope fractionation in refractory inclusions: Tracers of condensation and inheritance in the early solar protoplanetary disk. *Earth and Planetary Science Letters*, *472*, 277–288. https://doi.org/10.1016/j.epsl.2017.05.002

Skulan, J., DePaolo, D. J., & Owens, T. L. (1997). Biological control of calcium isotopic abundances in the global calcium cycle. *Geochimica et Cosmochimica Acta*, *61*(12), 2505–2510. https://doi.org/10.1016/s0016-7037(97)00047-1

Sobolev, A. V., Migdisov, A. A., & Portnyagin, M. V. (1996). Incompatible element partitioning between clinopyroxene and basalt liquid revealed by the study of melt inclusions in minerals from Troodos lavas, Cyprus. *Petrology*, *4*, 307–317.

Sossi, P. A., Foden, J. D., & Halverson, G. P. (2012). Redox-controlled iron isotope fractionation during magmatic differentiation: An example from the Red Hill intrusion, S. Tasmania. *Contributions to Mineralogy and Petrology*, *164*(5), 757–772. https://doi.org/10.1007/s00410-012-0769-x

Teng, F.-Z., Dauphas, N., & Helz, R. T. (2008). Iron isotope fractionation during magmatic differentiation in Kilauea Iki lava lake. *Science*, *320*(5883), 1620–1622. https://doi.org/10.1126/science.1157166

Teng, F.-Z., Dauphas, N., Helz, R. T., Gao, S., & Huang, S. (2011). Diffusion-driven magnesium and iron isotope fractionation in Hawaiian olivine. *Earth and Planetary Science Letters*, *308*(3–4), 317–324. https://doi.org/10.1016/j.epsl.2011.06.003

Teng, F.-Z., Li, W.-Y., Ke, S., Marty, B., Dauphas, N., Huang, S., et al. (2010). Magnesium isotopic composition of the earth and chondrites. *Geochimica et Cosmochimica Acta*, *74*(14), 4150–4166. https://doi.org/10.1016/j.gca.2010.04.019

Teng, F.-Z., Wadhwa, M., & Helz, R. T. (2007). Investigation of magnesium isotope fractionation during basalt differentiation: Implications for a chondritic composition of the terrestrial mantle. *Earth and Planetary Science Letters*, *261*(1–2), 84–92. https://doi.org/10.1016/j.epsl.2007.06.004

Teplow, W., Marsh, B. D., Hulen, J., Spielman, P., Kaleikini, M., Fitch, D., & Rickard, W. (2009). Dacite melt at the Puna geothermal venture wellfield, big island of Hawaii. *Geothermal Research Conference Transactions*, *33*, 989–994.

Tomascak, P. B., Tera, F., Helz, R. T., & Walker, R. J. (1999). The absence of lithium isotope fractionation during basalt differentiation: New measurements by multicollector sector ICP-MS. *Geochimica et Cosmochimica Acta*, *63*(6), 907–910. https://doi.org/10.1016/s0016-7037(98)00318-4

Valdes, M. C., Moreira, M., Foriel, J., & Moynier, F. (2014). The nature of Earth's building blocks as revealed by calcium isotopes. *Earth and Planetary Science Letters*, *394*, 135–145. https://doi.org/10.1016/j.eps1.2014.02.052

Walter, M. J. (1998). Melting of garnet peridotite and the origin of komatiite and depleted lithosphere. *Journal of Petrology*, *39*(1), 29–60. https://doi.org/10.1093/petroj/39.1.29

Wang, W., Zhou, C., Qin, T., Kang, J.-T., Huang, S., Wu, Z., & Huang, F. (2017). Effect of Ca content on equilibrium Ca isotope fractionation between orthopyroxene and clinopyroxene. *Geochimica et Cosmochimica Acta*, *219*, 44–56. https://doi.org/10.1016/j.gca.2017.09.022

Wombacher, F., Eisenhauer, A., Heuser, A., & Weyer, S. (2009). Separation of Mg, Ca and Fe from geological reference materials for stable isotope ratio analyses by MC-ICP-MS and double-spike TIMS. *Journal of Analytical Atomic Spectrometry*, *24*(5), 627–636. https://doi.org/10.1039/B820154D

Workman, R. K., & Hart, S. R. (2005). Major and trace element composition of the depleted MORB mantle (DMM). *Earth and Planetary Science Letters*, *231*(1–2), 53–72. https://doi.org/10.1016/j.epsl.2004.12.005

Wu, Z., Huang, F., & Huang, S. (2015). Isotope fractionation induced by phase transformation: First-principles investigation for Mg_2SiO_4. *Earth and Planetary Science Letters*, *409*, 339–347. https://doi.org/10.1016/j.epsl.2014.11.004

Young, E. D., Manning, C. E., Schauble, E. A., Shahar, A., Macris, C. A., Lazar, C., & Jordan, M. (2015). High-temperature equilibrium isotope fractionation of non-traditional stable isotopes: Experiments, theory, and applications. *Chemical Geology*, *395*, 176–195. https://doi.org/10.1016/j.chemgeo.2014.12.013

Zhao, X., Zhang, Z., Huang, S., Liu, Y., Li, X., & Zhang, H. (2017). Coupled extremely light Ca and Fe isotopes in peridotites. *Geochimica et Cosmochimica Acta*, *208*, 368–380. https://doi.org/10.1016/j.gca.2017.03.024

Zhou, C., Kang, J., Wang, W., Wu, Z., & Huang, F. (2016). First-principles calculations of equilibrium calcium isotope fractionation among Ca-bearing minerals. Paper presented at the 2016 AGU Fall Meeting, San Francisco.

Zhu, H., Liu, F., Li, X., Wang, G., Zhang, Z., & Sun, W. (2018). Calcium isotopic compositions of normal mid-ocean ridge basalts from the southern Juan de Fuca ridge. *Journal of Geophysical Research: Solid Earth*, *123*, 1303–1313. https://doi.org/10.1002/2017JB014699

Zhu, H. L., Zhang, Z. F., Wang, G. Q., Liu, Y. F., Liu, F., Li, X., & Sun, W. D. (2016). Calcium isotopic fractionation during ion-exchange column chemistry and thermal ionisation mass spectrometry (TIMS) determination. *Geostandards and Geoanalytical Research*, *40*(2), 185–194. https://doi.org/10.1111/j.1751-908X.2015.00360.x

Zhu, P., & Macdougall, J. D. (1998). Calcium isotopes in the marine environment and the oceanic calcium cycle. *Geochimica et Cosmochimica Acta*, *62*(10), 1691–1698. https://doi.org/10.1016/s0016-7037(98)00110-0